

tem size (e.g., $M_n \sim 5000$) the boundary conditions do not affect the results. In the subsequent discussions, we will mainly present the results obtained using the fixed boundary conditions, under which M_n denotes the number of free (non-fixed) nodes.

Next, N_p active particles (e.g., congruent spheres) are introduced in the network such that each particle occupies a randomly selected un-occupied node (i.e., each node can be occupied by only one particle). The *number density* ρ of the particles is defined as $\rho = N_p/M_n$, i.e., the fraction of nodes occupied by the active particles. Each particle can generate a contraction, which pulls all of the bonds connected to the node it occupies towards the particle center (i.e., the node) by a fixed amount δl , leading to different pulling forces in the bonds and thus, a force network in the system. We consider the particles can “migrate” from its original node to an un-occupied neighboring node following local durotaxis, i.e., along the bond with the highest stiffness, which is also the bond that carries the largest pulling force among all neighboring bonds (see Fig. 1 for illustration). The diameter of the particles is not essential in our model and thus, is not explicitly considered here.

The bonds of the network are modeled as elastic elements with only non-zero stretching modulus E_s and free to rotate at the nodes. An active particle can generate pulling forces in the bonds connected to the node it occupies by contraction, i.e., δl . This contraction leads to a strain $\epsilon_i = \delta l/l_i$ in the bond i with original length l_i , and thus, a pulling force $f_s = E_s A \delta l/l_i$, where A is an effective cross-sectional area of the bonds. These pulling forces impose force boundary conditions for the ECM network, and the force-balance network configuration is obtained using an iterative force-based relaxation approach [22].

We note that many factors can affect the interactions between the dynamic force network and the collective dynamics of the active particles in our APN model. These may include the geometry/topology and mechanical properties of the network, as well as the number density, spatial distribution and the contractibility (i.e., δl) of the active particles. In this work, we mainly focus on disordered isostatic networks (i.e., $Z = 6$) derived from maximally random jammed packings of congruent hard spheres [25]. It is straightforward to generalize this study to random network models derived from confocal images of collagen gels [26]. In addition, we use simple linear elastic network models (see Methods). This allows us to investigate the system in the elastic regime [27], in which the force network is mainly determined by the number density and spatial distribution of the active particles, and largely independent of particle contractibility. Our model can readily incorporate more realistic mechanical models for the ECM, taking into account non-linear responses of the fibers [28, 29] and plasticity [13]. Moreover, in an actual cell-ECM system, the cell migration might not be sensitive to individual stiffer fibers, but determined by certain meso-scale stiff structures emerged

due to cell remodeling, such as bundles of high-stress fibers. Nonetheless, we believe that the general organizational principles of active particles on random networks obtained here are relevant to and can provide insights on the actual cell-ECM systems.

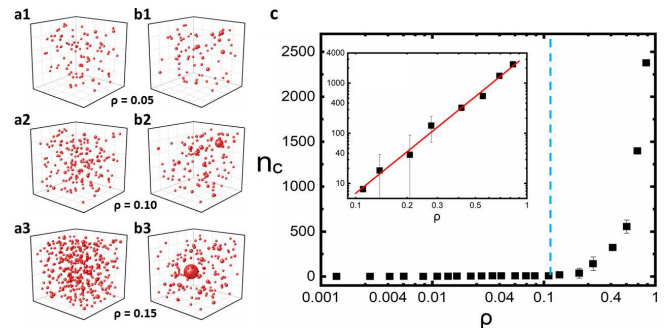


FIG. 2: (a) Initial distribution of clusters formed by randomly placed active particles on the network for different number densities ρ . In these plots, a cluster is represented by a sphere for better visualization with the center coinciding with the center of the cluster and the radius representing the cluster size. (b) Distribution of clusters in the final state of the APN system. As ρ increases, the majority of particles tend to aggregate into a single large cluster in the system. (c) The maximal cluster size n_c (see definition in the text) as a function of ρ . A transition behavior is apparent as ρ approaches $\rho_c \approx 0.114$ from below (indicated by the dashed line). The inset shows the log-scale plot of n_c for $\rho > \rho_c$. The statistics are obtained by averaging over 20 independent simulations.

Dynamic phase transition in the APN system:

We now describe the observed collective dynamics of the active particles on the random networks. In our simulations, we systematically vary the particle number density $\rho \in (0.05, 0.95)$. For each ρ , the particles are initially randomly introduced in the network and the system is allowed to evolve according to the aforementioned APN dynamics. At low densities (i.e., $\rho < \rho_c \approx 0.114$), the particles rapidly aggregate into multiple isolated small clusters, which are randomly distributed within the ECM (see Fig. 2a and 2b). Here, we consider two particles belong to the same “cluster” if they occupy the two nodes connected by the same bond. As ρ approaches ρ_c from below, the maximal cluster size n_c (i.e., the number of particles in the largest cluster of the system) increases dramatically (see Fig. 2c), indicating the majority of the particles are connected to form a single large cluster in the system.

In addition, we find that the isolated small clusters associated with $\rho < \rho_c$ are stationary, i.e., the particles in the clusters either do not move at all or hop between two adjacent nodes (typically at the boundary of a cluster). On the other hand, the dominant large clusters formed for $\rho > \rho_c$ undergo constant dynamic reorganization. To further quantify the dynamics of the clusters, we count the number of distinct nodes m_s visited by a particle dur-

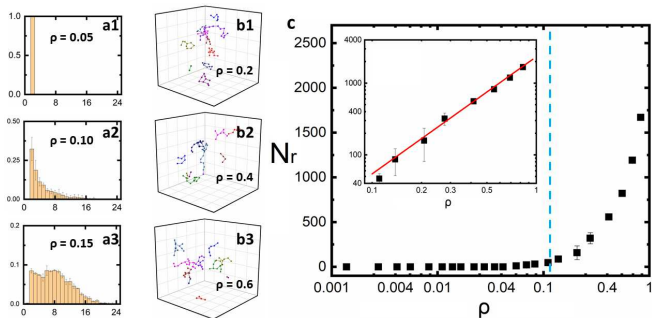


FIG. 3: (a) Statistics of the number of distinct nodes m_s visited by a particle for $s = 24$ successive steps for different number densities ρ . As ρ approaches ρ_c from below, a subset of highly dynamic particles emerge which are able to visit many distinct nodes for a given number of steps and are referred to as “radicals”. (b) Representative trajectories for 10 randomly selected radicals (i.e., highly dynamic particles) for different ρ . (c) The number of radicals N_r as a function of ρ , which exhibits a clear transition at $\rho_c \approx 0.114$ (indicated by the dashed line). This is consistent with the transition observed in the maximal cluster size n_c as ρ increases (see Fig. 2c). The inset shows the log-scale plot of N_r for $\rho > \rho_c$.

ing a total of s successive steps. The collected statistics for different particle densities are shown in Fig. 3a. We note that the m_s statistics shown in Fig. 3a does not depend on s and we have used $s = 24$ here.

It can be seen from Fig. 3a that for small ρ , a particle can only visit one or two nodes, respectively indicating that the particle does not move or can hop between two adjacent nodes. As ρ approaches ρ_c from below, although the majority of particles are localized (indicated by the peak in the m_s statistics associated with small node numbers), a subset of highly dynamic particles emerge which are able to visit many distinct nodes for a given number of steps (indicated by the emergence of the second peak associated with large node numbers in the m_s statistics). We refer to these highly dynamic particles as “radicals”, i.e., those do not possess a periodic hopping pattern over all a finite number nodes. The trajectory of a small number of randomly selected radicals are shown in Fig. 3b for different ρ values. Fig. 3c shows the number of radicals N_r as a function of ρ . It can be seen that N_r exhibits a clear transition as ρ increases towards ρ_c . This is consistent with the transition observed in the maximal cluster size n_c as ρ increases (see Fig. 2c).

The above analysis suggests that the system possesses a phase-transition-like behavior, as the particle number density ρ increases, from an “absorbing” state in which the particles segregate into small isolated stationary clusters, to a “active” state, in which the majority of particles join in a single large dynamic cluster. This transition is also quantitatively manifested in the maximal cluster size $n_c(\rho)$ (Fig. 2c) and radial number $N_r(\rho)$ (Fig. 3c) as ρ increases towards $\rho_c \approx 0.114$. In particular, our scaling analysis shows that as ρ_c is approached from above,

$n_c \sim (\rho - \rho_c)^\alpha$, where the critical exponent $\alpha \approx 6.6 \pm 0.1$. In addition, we find that $N_r \sim (\rho - \rho_c)^\beta$, where the critical exponent $\beta \approx 1.63 \pm 0.04$. The numerical values of α , β and ρ_c are obtained by fitting the simulation data. We also note that the ρ_c value is much lower than the site percolation threshold for the network (≈ 0.310) [30]. The absorbing-to-active transition has also been observed in a wide spectrum of “random-organizing” physical systems, such periodically driven colloids [31–33], granular materials and amorphous solids [34–36], vortices [37] and skyrmion systems [38].

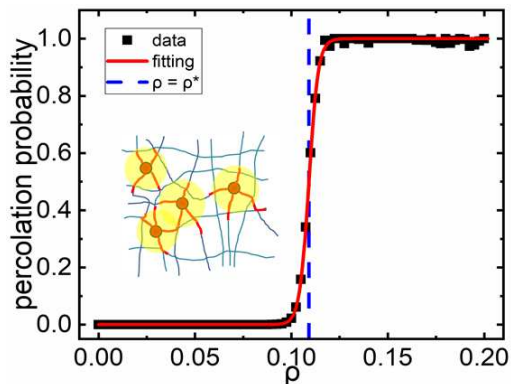


FIG. 4: Percolation probability analysis indicates a percolation transition of overlapping influence spheres with radius $R_I = 0.104L$ at $\rho^* \approx 0.109$, which agrees well with the critical density $\rho_c \approx 0.114$ for the dynamic phase transition in the APN system. Inset: Schematic illustration of the concept of the influence region (yellow circles), characterizing the range of the pulling forces (red) due to particle (red) contraction.

Influence sphere due to active pulling forces: We now investigate the mechanisms for the observed transition. Once a particle pulls the fibers, a stress gradient is built up surrounding this particle. When another particle “senses” the pulling force [21], it will tend to move up the stress gradient towards the contracting particle due to local durotaxis. This would lead to an effective mutual pulling between the particles.

It is reasonable to assume that the pulling forces generated by a specific particle can only influence other particles within a certain distance R_I . Due to the intrinsic network heterogeneity, R_I may vary for different particles. Here, we take a “mean-field” approach and assign the same effective R_I to all the particles in the system and introduce the concept of the *influence sphere*, which is a spherical region with radius R_I centered at a contractile particle (see the inset of Fig. 4).

The influence-sphere radius R_I is estimated from the cluster statistics of the APN systems at low ρ , i.e., those containing multiple small isolated stationary clusters in the final state. This is based on the assumption at low ρ , only particles which are within the influence region of one another would eventually aggregate. In particular, we first identify the particles within the same cluster in the final state of the system. Then the system

is “re-winded” to the initial state, and the intra-cluster nearest-neighbor distances d_n are computed for all clusters. We then use the mean nearest-neighbor distance \bar{d}_n to estimate $R_I \approx 0.104L$ (where L is the linear system size), which is roughly twice of the average fiber length (see SI for fiber length distributions).

Mean field theory: Percolation of influence sphere: We now investigate the percolation of the influence spheres as ρ increases. For a given ρ , we randomly place particles on the ECM network. Instead of allowing the particles to move according to the APN dynamics, we place a virtual sphere with radius $R_I = 0.104L$ at each particle, representing the influence spheres. We subsequently identify the clusters formed by the influence spheres, based on which the percolation of the system can be determined.

Fig. 4 shows the percolation probability analysis for the system [39] (see SI for details), from which a percolation transition and the associated critical density (i.e., percolation threshold) $\rho^* \approx 0.109$ can be clearly identified. Interestingly, the percolation transition of the influence spheres coincides with the dynamic transition of the active particles at $\rho_c \approx 0.114$. This suggests that the dynamic transition of the active particles from the “absorbing” state to the “active” state is underlaid by and can be understood as the percolation transition of the influence spheres.

We also investigate the collective dynamics of active particles on other network models, including the networks derived from the diamond lattice, as well as random networks reconstructed based on confocal images (see SI for details). We find that although the critical transition density ρ_c depends on the geometry and topology of the networks, the dynamic transition and the aggregation behaviors of the active particles occur in all

of the studied model networks. This suggests the feedback loop between the evolving force network and particle dynamics provides a robust mechanism for regulating collective migratory behaviors. In future work, we will also explore the effects of fiber alignment and external mechanical cues.

Finally, we emphasize again that this minimal model does not take into account crucial mechanisms in actual cell migration such as ECM remodeling (e.g., orientation, bundling and degradation) and cell-cell adhesion. Interestingly, our studies indicate that, at least for the APN systems, the local durotaxis for the active particles is sufficient to induce and stabilize aggregations, even without adhesion. Nonetheless, we expect that the insights on the collective behaviors of active particles regulated by the dynamically evolving force network obtained here are helpful in understanding the collective dynamics emerged in actual multi-cellular-ECM systems, as well as in other active-particle systems dominated by environment-mediated particle-particle interactions.

Acknowledgments

H. N., Y. Z., Y. J. thank Arizona State University for the generous start-up funds and the University Graduate Fellowship. W.X. was supported by the National Natural Science Foundation of China (Grant No. 11772120). C. E and B. S. thank the support from the Scialog Program sponsored jointly by Research Corporation for Science Advancement and the Gordon and Betty Moore Foundation. B. S. is partially supported by the Medical Research Foundation of Oregon and SciRIS-II award from Oregon State University and by the National Science Foundation Grant PHY-1400968.

-
- [1] Aman, A. and T. Piotrowski, Cell migration during morphogenesis. *Developmental Biology*, 2010. 341(1): p. 20-33.
 - [2] Friedl, P. and D. Gilmour, Collective cell migration in morphogenesis, regeneration and cancer. *Nature Reviews Molecular Cell Biology*, 2009. 10(7): p. 445.
 - [3] Vaezi, A., C. Bauer, V. Vasioukhin, and E. Fuchs, Actin cable dynamics and Rho/Rock orchestrate a polarized cytoskeletal architecture in the early steps of assembling a stratified epithelium. *Developmental cell*, 2002. 3(3): p. 367-381.
 - [4] Werner, S., T. Krieg, and H. Smola, Keratinocytefibroblast interactions in wound healing. *Journal of Investigative Dermatology*, 2007. 127(5): p. 998-1008.
 - [5] Ridley, A.J., M.A. Schwartz, K. Burridge, R.A. Firtel, M.H. Ginsberg, G. Borisy, J.T. Parsons, and A.R. Horwitz, Cell migration: integrating signals from front to back. *Science*, 2003. 302(5651): p. 1704-1709.
 - [6] Friedl, P. and E.-B. Brcker, The biology of cell locomotion within three-dimensional extracellular matrix. *Cellular and molecular life sciences CMLS*, 2000. 57(1): p. 41-64.
 - [7] Szurmant, H. and G.W. Ordal, Diversity in chemotaxis mechanisms among the bacteria and archaea. *Microbiology and Molecular Biology Reviews*, 2004. 68(2): p. 301-319.
 - [8] Sunyer, R., V. Conte, J. Escribano, A. Elosegui-Artola, A. Labernadie, L. Valon, D. Navajas, J.M. Garca-Aznar, J.J. Muoz, and P. Roca-Cusachs, Collective cell durotaxis emerges from long-range intercellular force transmission. *Science*, 2016. 353(6304): p. 1157-1161.
 - [9] Carter, S.B., Haptotaxis and the mechanism of cell motility. *Nature*, 1967. 213(5073): p. 256.
 - [10] Provenzano, P.P., D.R. Inman, K.W. Eliceiri, S.M. Trier, and P.J. Keely, Contact guidance mediated three-dimensional cell migration is regulated by Rho/ROCK-dependent matrix reorganization. *Biophysical Journal*, 2008. 95(11): p. 5374-5384.
 - [11] Lecuit, T., P.-F. Lenne, and E. Munro, Force generation, transmission, and integration during cell and tissue morphogenesis. *Annual Review of Cell and Developmental Biology*, 2011. 27: p. 157-184.

- [12] Jones, C.A., M. Cibula, J. Feng, E.A. Krnacik, D.H. McIntyre, H. Levine, and B. Sun, Micromechanics of cellularized biopolymer networks. *Proceedings of the National Academy of Sciences*, 2015. 112(37): p. E5117-E5122.
- [13] Kim, J., J. Feng, C.A. Jones, X. Mao, L.M. Sander, H. Levine, and B. Sun, Stress-induced plasticity of dynamic collagen networks. *Nature Communications*, 2017. 8(1): p. 842.
- [14] Chen, S., Xu, W., Kim, J., Nan, H., Zheng, Y., Sun, B., and Jiao, Y, Novel Inverse Finite-Element Formulation for Reconstruction of Relative Local Stiffness in Heterogeneous Extra-cellular Matrix and Traction Forces on Active Cells. *Physical biology*, 2019. 16: p 036002.
- [15] Heussinger, C. and Frey, E., Force distributions and force chains in random stiff fiber networks. *Euro Physics Journal E*, 2007. 24: p 4753.
- [16] Grinnell, F. and W.M. Petroll, Cell motility and mechanics in three-dimensional collagen matrices. *Annual Review of Cell and Developmental Biology*, 2010. 26: p. 335-361.
- [17] Han, Y.L., P. Ronceray, G. Xu, A. Malandrino, R.D. Kamm, M. Lenz, C.P. Broedersz, and M. Guo, Cell contraction induces long-ranged stress stiffening in the extracellular matrix. *Proceedings of the National Academy of Sciences*, 2018, 115: p. 4075-4080.
- [18] Ma, X., M.E. Schickel, M.D. Stevenson, A.L. Sarang-Sieminski, K.J. Gooch, S.N. Ghadiali, and R.T. Hart, Fibers in the extracellular matrix enable long-range stress transmission between cells. *Biophysical Journal*, 2013. 104(7): p. 1410-1418.
- [19] Ronceray, P., C.P. Broedersz, and M. Lenz, Fiber networks amplify active stress. *Proceedings of the National Academy of Sciences*, 2016. 113(11): p. 2827-2832.
- [20] Wang, H., A. Abhilash, C.S. Chen, R.G. Wells, and V.B. Shenoy, Long-range force transmission in fibrous matrices enabled by tension-driven alignment of fibers. *Biophysical Journal*, 2014. 107(11): p. 2592-2603.
- [21] Beroz, F., L.M. Jawerth, S. Mnster, D.A. Weitz, C.P. Broedersz, and N.S. Wingreen, Physical limits to biomechanical sensing in disordered fibre networks. *Nature Communications*, 2017. 8: p. 16096.
- [22] Liang, L., C. Jones, S. Chen, B. Sun, and Y. Jiao, Heterogeneous force network in 3D cellularized collagen networks. *Physical biology*, 2016. 13(6): p. 066001.
- [23] Popkin, G., *The Physics of Life*. *Nature*, 2016. 529: p 16.
- [24] Bechinger, C., Di Leonardo, R., Lowen, H., Reichhardt, C., Volpe, G., and Volpe, G. *Active Particles in Complex and Crowded Environments*. *Reviews of Modern Physics*, 2016. 88: p 045006.
- [25] Torquato, S., Truskett, T. M., and Debenedetti, P. G., Is Random Close Packing of Spheres Well Defined? *Physical Review Letters*, 2000. 84: p 2064.
- [26] Nan, H., L. Liang, G. Chen, L. Liu, R. Liu, and Y. Jiao, Realizations of highly heterogeneous collagen networks via stochastic reconstruction for micromechanical analysis of tumor cell invasion. *Physical Review E*, 2018. 97(3): p. 033311.
- [27] Head, D.A., Levine, A.J., and MacKintosh, F.C., Mechanical response of semiflexible networks to localized perturbations. *Physical Review E*, 2005. 72: p 061914.
- [28] Shokef, Y., and Safran, S.A., Scaling laws for the response of nonlinear elastic media with implications for cell mechanics. *Physical Review Letters*, 2012. 108: p 178103.
- [29] Steinwachs, J., Metzner, C., Skodzek, K., et. al. Three-dimensional force microscopy of cells in biopolymer networks, *Nature Method*, 2016. 13: p 171-6.
- [30] Powell, M. J., Site Percolation in Randomly Packed Spheres. *Physical Review B*, 1979. 20: p 41944198
- [31] Corte, L., Chaikin, P., Gollub, J. P. and Pine, D., Random organization in periodically driven systems. *Nat. Phys.* 4, 420-424 (2008).
- [32] Menon, G. I. and Ramaswamy, S. Universality class of the reversible-irreversible transition in sheared suspensions. *Phys. Rev. E* 79, 061108 (2009).
- [33] Franceschini, A., Filippidi, E., Guazzelli, E. and Pine, D. J. Transverse alignment of fibers in a periodically sheared suspension: an absorbing phase transition with a slowly varying control parameter. *Phys. Rev. Lett.* 107, 250603 (2011).
- [34] Regev, I., Weber, J., Reichhardt, C., Dahmen, K. A. and Lookman, T. Reversibility and criticality in amorphous solids. *Nat. Commun.* 6, 8805 (2015).
- [35] Royer, J. R. and Chaikin, P. M. Precisely cyclic sand: Self-organization of periodically sheared frictional grains. *Proc. Natl. Acad. Sci. U.S.A* 112, 49-53 (2015).
- [36] Milz, L. and Schmiedeberg, M. Connecting the random organization transition and jamming within a unifying model system. *Phys. Rev. E* 88, 062308 (2013).
- [37] Mangan, N., Reichhardt, C. and Reichhardt, C. O. Reversible to irreversible ow transition in periodically driven vortices. *Phys. Rev. Lett.* 100, 187002 (2008).
- [38] Brown, B., Reichhardt, C. and Reichhardt, C. Reversible to irreversible transitions in periodically driven skyrmion systems. *New J. Phys.* 21, 013001 (2019).
- [39] Xu, W., Su, X., and Jiao, Y., Continuum Percolation of Congruent Overlapping Spherocylinders, *Physical Review E*, 2016. 94: p 032122.